

## High detectivity uncooled thermopile IRFPA chip prepared by surface micro-machining

A. Ihring, E. Kessler, U. Dillner, F. Hänschke, U. Schinkel, H.-G. Meyer

*Institute of Photonic Technology, Albert-Einstein-Str. 9, D-07745 Jena, Germany*

### Abstract

Thermopile detectors are particularly well suited for spectral imaging, space science applications, track recording, presence detection and applications with low energy consumption. The purpose of this work is the fabrication of a surface micromachined 2-D high detectivity infrared thermopile array using a thermoelectrically effective  $\text{Bi}_{0.87}\text{Sb}_{0.13}\text{-Sb}$  thermopair materials combination. The thermopile array comprises  $8 \times 8$  pixels with an active area of 100 microns in square, which are wired directly. Each pixel consists of eight  $\text{Bi}_{0.87}\text{Sb}_{0.13}\text{-Sb}$  thermocouples arranged on top of each other, which are isolated and passivated by a thin layer of  $\text{Si}_x\text{N}_y$ . The intrinsic stress of  $\text{Si}_x\text{N}_y$  layers is well suited to avoid a sticking effect or an excessive deflection of the absorber area after removing the sacrificial layer. Thermopile structure and absorber area are manufactured upon a sacrificial layer based on polyimide. This organic material can be structured well in an oxygen rf-plasma process with a high selectivity to the membrane material. After removing the sacrificial layer in an isotropic plasma process, membranes are free-standing and suspended by four spiral legs. Due to their long thermal paths and low thermal conductivity these legs provide a high thermal gradient between the absorber area, heated by an incoming infrared radiation, and the substrate surface, which acts as a heat sink.

Thermoelectric layers as well as wiring layers were patterned almost exclusively by lift-off technique in order to obtain very small structure dimension with high reliability as well as high integration level. Detectors can be equipped with two absorber types. For broadband application a well suited colloidal silver black layer absorber is available. A second option is a quarter wavelength arrangement with a absorption coefficient of 0.88 suited for the 8-14  $\mu\text{m}$  band. A higher absorption coefficient was obtained with the silver black layer absorber over a broad spectral range. This layer was deposited in an evaporation process after the sacrificial layer was removed. The amount of absorption depends on the deposited thickness and can be well controlled by the process. The detectivity of so manufactured IRFPAs is about  $1 \cdot 10^9 \text{ cmHz}^{-1/2}/\text{W}$  exceeding most of the state-of-the-art thermopile detectors. The time constant was measured to be 36 ms.

### Keywords

Thermoelectric focal plane array, High detectivity, Surface micromachining, Infrared absorber, Colloidal silver black layer

### 1. Introduction

Recently, a lot of research and development has been done in the field of uncooled infrared focal-plane arrays (FPA) with thermopiles [1-3] as well as bolometers [4]. Thermopiles as thermal detectors are characterized by their simplicity and ruggedness of construction corresponding to low cost. They exhibit a uniform broadband response over the infrared spectrum, can be operated without cooling and generate a signal voltage, which is strictly proportional to the incoming radiation over many orders of magnitude and, moreover, insensitive to substrate temperature variations. In addition, they require neither an electrical bias nor an optical chopper and do not generate  $1/f$  noise. Therefore, thermopile detectors are well suited for spectral imaging, space applications, track recording, presence detection and applications requiring low energy consumption. Both detector types, thermopile as well as bolometers, have been manufactured by either bulk- or surface micromachining. For surface micromachined sensor arrays offering a high responsivity and integration level, however, a vacuum packaging is indispensable due to the small distance between absorber area and substrate surface.

Most IRFPAs have been realized by applying CMOS compatible processes [2,3], however, for a higher detectivity it is advantageous to use V-VI-alloys, e.g., a materials combination of n-type  $\text{Bi}_{0.87}\text{Sb}_{0.13}$  and p-type Sb due to their relatively high thermoelectric efficiency and low thermal conductivity. Furthermore, to

obtain a high detectivity, it is necessary to realize a low thermal conductivity of all isolation and passivation layers.

An important part of all thermal infrared detectors including thermopiles as well as bolometers is the absorber area, which converts the incoming infrared radiation into heat and generates a thermal gradient. For a high thermoelectric output voltage it is crucial to realize an absorber with a high absorption coefficient. Many thermal infrared detectors are fabricated with colloidal black layers [2,5] as well as quarter wavelength structures [6]. Recently, a carbon nanotube absorber for infrared detectors has been developed [7]. This absorber type as well as the colloidal metal black layers provide a very large absorbing surface for incoming radiation and contribute to a high detector performance.

## 2. Fabrication

### 2.1 Surface micromachining and sacrificial layer

For manufacturing the FPA a surface micromachining technology has been used. So a higher integration level can be realized compared to the analogous detector arrays fabricated by bulk micromachining. For realization of a well-defined distance between the active absorber area and the substrate surface a sacrificial polyimide layer of 2.5  $\mu\text{m}$  *Polyimide 2555* was spun on. After the annealing process at 210  $^{\circ}\text{C}$  the polyimide was structured in a dry RIE process with an oxygen plasma against a patterned photoresist *AZ4562* mask layer of 4  $\mu\text{m}$  in thickness. After this process the mask layer was removed in acetone. After this, rectangular plateaus with slanted sides were obtained.

The slanted sides are mandatory for the reliability of metallization layers as well as isolation layers, which are structured from the substrate surface to the higher level upon the sacrificial layer. The structured polyimide layer was subsequently covered with a silicon nitride layer. This silicon nitride layer serves as a carrier membrane for thermopiles as well as absorber area.

At the end of fabrication process, the sacrificial layer has to be removed completely in a remote RIE process by using an oxygen plasma. Thus, a freestanding pixel area is obtained. The remote process is a very isotropic dry etching process and has a high selectivity to other exposed layers, i.e. silicon nitride.

### 2.2 Wiring layer and diffusion barrier

The wiring layer of the FPA was realized using gold, because it has a very high conductivity, electrical as well as thermal, and it is highly selective during structuring processes of other materials within the process chain. Each pixel was wired directly. For structuring of the wiring layer a lift-off process with a patterned photoresist layer of *AZ5214E* was applied. The lift-off layer was patterned by a wafer stepper and image reversal process to obtain undercut structures. So, high precisely structured layers were realized. The E-gun evaporated gold-layer had a thickness of 120 nm. The connecting lines of each pixel between the bonding area at the edge of an array and the associated thermopile have a width of 2  $\mu\text{m}$ .

The wiring layer, which is connected directly to the diffusion barrier, was structured on top of the silicon nitride covered sacrificial layer. The diffusion barrier between the wiring layer and the thermoelectric materials layers, BiSb as well as Sb, of each thermopile was made of nickel. Nickel is one of commonly used

materials as diffusion barrier, i.e. in thermoelectric power generators. The Ni contacts, with a thickness of 130 nm, serve as intermediate connecting areas between Au/BiSb as well as Au/Sb and BiSb/Sb interconnects, as it is shown in Fig.1. Just as gold, nickel was deposited in an E-gun evaporation process and structured by using the lift-off process described above.

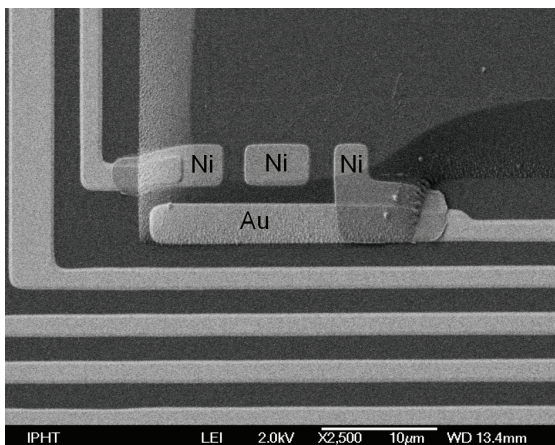


**Fig.1:** SEM picture of gold connecting lines and nickel diffusion barrier areas on top of the sacrificial layer with slanted sides.

Without the Ni barrier a material diffusion of BiSb as well as Sb was observed at the contact area with gold at temperatures over 130  $^{\circ}\text{C}$  after several minutes. Because the subsequent process steps as well as tempering steps partly include temperatures over 120  $^{\circ}\text{C}$ , the implementation of a nickel diffusion barrier was indispensable.

### 2.3 Thermopile and thermoelectric materials

For the high detectivity infrared array a materials combination of a bismuth-antimony alloy and antimony has been used. This material combination is well suited for sensor applications from room temperature up to 80 °C. Each thermopile consists of eight thermocouples of n-type BiSb and p-type Sb, which are arranged on top of each other and connected in series. The Seebeck coefficient  $S$  or thermopower of these thin films is  $-100 \mu\text{VK}^{-1}$  for BiSb and  $35 \mu\text{VK}^{-1}$  for Sb [8]. For the optimization of thermopiles the thermoelectric figure of merit  $Z$  of a material as well as of a n-type/p-type materials combination is one of the most important material parameters. For a particular material  $Z$  is defined as:

$$Z = \frac{S^2 \sigma}{\lambda}$$

Here  $S$  denotes the Seebeck coefficient,  $\sigma$  the electrical conductivity and  $\lambda$  the thermal conductivity of the material.

To increase the detectivity of the thermopile, the optimum BiSb alloy, i.e.  $\text{Bi}_{0.87}\text{Sb}_{0.13}$  with a thermoelectric figure of merit of  $0.5 \cdot 10^{-3} \text{K}^{-1}$  [9], was used as n-type material. The 150 nm thin Sb-layer as well as the 350 nm thin BiSb-layer were deposited at room temperature and structured via lift-off technique by using  $1.5 \mu\text{m}$  photoresist *AZ5214E* as masking layer. For a better electrical contact between nickel and the deposited thermoelectric material, BiSb as well as Sb, a dry etching step with argon ions (IBE) by using an ion beam source was accomplished. During this process the contact area surface is cleaned from contaminations. Thus, the electrical contact between the adjacent materials is improved, thereby reducing the contact resistance to a minimum. The IBE process as well as the following deposition process were realized seamlessly under vacuum condition. The Sb-layer as well as the BiSb-layer were thermally evaporated by using a thin sheet of tantalum with a dimple. To control the deposition thickness during the evaporation process an oscillating crystal equipment was used.

Because of the lower thickness of the Sb-layer compared to the BiSb-layer it is technologically advantageous to deposit the antimony layer at first. As shown in Fig.2, the inner as well as the outer nickel contacts are connected by the Sb-layer spirally arranged around the absorber area.

During operation, the inner contacts will be heated by the absorber area, which converts the incoming radiation into heat. The outer contacts, which are connected to the electrical wiring layer, are located on the silicon wafer serving as a heat sink. Due to the thermal gradient a signal voltage will be generated, which is strictly proportional to the incoming radiation over many orders of magnitude.

To avoid electrical short circuits between the Sb- and the BiSb-layer an isolation layer of 250 nm thin silicon nitride was deposited. To ensure electrical contact between nickel areas and the BiSb-layer the isolation layer was opened in the corresponding contact areas by using a RIE-ICP dry etching process with a gas mixture of  $\text{CHF}_3/\text{CF}_4/\text{He}$ . During the etch process the substrate was tempered at 15 °C by using back-side helium cooling.

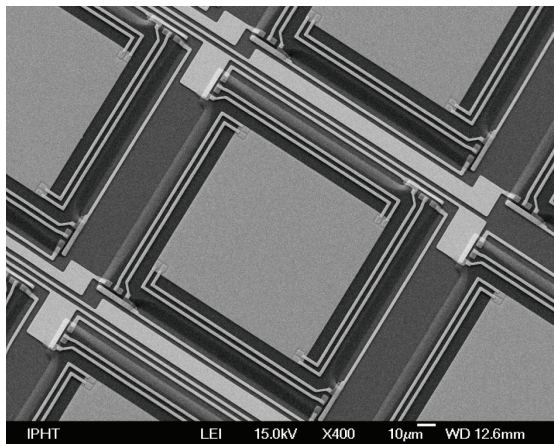


**Fig.2:** Pixel with structured Sb-layer upon the sacrificial layer, which connects inner and outer nickel contacts.

A structured photoresist layer of  $1.5 \mu\text{m}$  *AZ5214E* serving as a mask layer was removed completely by using acetone, followed by an oxygen plasma cleaning step after the structuring was finished.

For deposition of the second thermoelectric layer a further photoresist layer of  $1.5 \mu\text{m}$  *AZ5214E* was spun on and patterned with undercut structures. After structuring of the BiSb-layer, all thermocouples were electrically connected thus completing the thermopiles. Then the resistance of some thermopiles was measured by using test structures on the substrate. To facilitate test measurements with a wafer prober, contact pads of test structures were opened simultaneously during the RIE-ICP dry etching process of the isolation layer. The thermopile test structures had the same size as the pixel thermopiles and were evenly distributed over the whole substrate to control the influence of the thickness variation of the deposited Sb- as well as BiSb-layer in the middle and the boundary area of the substrate. The thickness variation de-

depends on the limited homogeneity of the evaporation process and can be measured indirectly by measuring the electrical resistance of the test structures. The electrical resistance was approximately 13 k $\Omega$  for test structures in the middle and 14 k $\Omega$  for test structures of the boundary area as expected for the given thermopile dimensions.

After electrical measurements a passivation layer of 350 nm Si<sub>x</sub>N<sub>y</sub> was deposited. Thus, the complete thermopile structure, diffusion barrier and wiring layer, was covered with Si<sub>x</sub>N<sub>y</sub> to avoid oxidation of the deposited materials as well as for optimal insulation.

#### 2.4 Stress-controlled free-standing membrane

The complete Si<sub>x</sub>N<sub>y</sub>-membrane of a FPA-pixel consists of three parts, the carrier membrane, the isolation layer and the passivation layer. In combination with the deposited thermoelectric structure the intrinsic stress of these layers is optimized to avoid sticking effects or excessive deflection of the fragile free-standing absorber area.

The Si<sub>x</sub>N<sub>y</sub>-layers were deposited by using a PECVD-ICP process with a gas mixture of (5%SiH<sub>4</sub>/95%He)/NH<sub>3</sub>/Ar. The advantage of using a PECVD process is the relatively low deposition temperature. Thus, high quality isolation and passivation layers with minimized residual thermal stress can be deposited on temperature-sensitive materials. To generate a homogeneous stress dispersion in a Si<sub>x</sub>N<sub>y</sub>-layer during the deposition, a substrate electrode with a helium backside cooling and in situ temperature measurement during the deposition process was used. Because the intrinsic stress of Si<sub>x</sub>N<sub>y</sub>-layers depends on the deposition temperature the controlling of the deposition temperature, which is one of the important process parameter concerning the deflection of the freestanding membrane, is indispensable.

The other crucial process parameter at a constant deposition temperature is the composition of the gas mixture. By a variation of the ratio between SiH<sub>4</sub> and NH<sub>3</sub> the nitrogen proportion of the deposited Si<sub>x</sub>N<sub>y</sub>-layer varies, too. Thus, a variation of intrinsic stress, tensile as well as compressive, can be realized at a given temperature.

The deposition of all fabricated Si<sub>x</sub>N<sub>y</sub>-layers was carried out at 130 °C. The gas flow of SiH<sub>4</sub>/He-mixture was kept constant at 145 sccm as well as the gas flow of 140 sccm Ar. The gas flow of NH<sub>3</sub> during the deposition of the carrier membrane was kept constant at 9.6 sccm. During the deposition of isolation and passivation layers the NH<sub>3</sub> gas flow was changed lightly and kept constant at 9.8 sccm. This results in a tensile stress of approximately 25 MPa for the carrier membrane and 40 MPa for the isolation layer as well as the passivation layer. This was determined in preliminary tests on a four inch one-side deposited silicon substrate by using a film measurement system *Tencor FLX-2900*, which allows the measurement of the substrate curvature caused by a deposited layer.

The variation of intrinsic stress for the optimized deflection of the absorber area was studied by a mechanical simulation of the given membrane structure using the finite element method (FEM) code *COMSOL*. Different deflections are shown in Fig.3. To avoid a sticking effect after sacrificial layer removing a concave deflection of the absorber area is necessary. The amount of intrinsic stress of the thermoelectric layers was determined in preliminary tests, similar to those of the Si<sub>x</sub>N<sub>y</sub>-layers, by depositing 4 inch silicon substrates with the thermoelectric material of the same thickness finally applied in the fabrication process of the FPA.

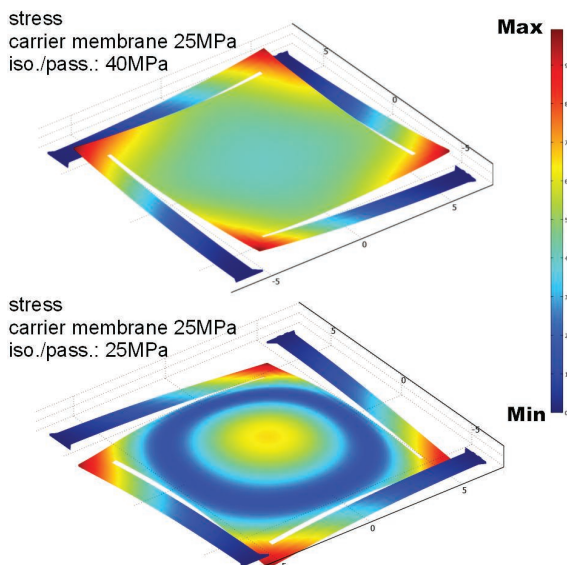


**Fig.3:** FEM simulation of the deflection of a FPA-pixel induced by intrinsic stress for two different values of the intrinsic stress in the isolation layer as well as passivation layer.

An intrinsic stress of 23 MPa tensile for the 350 nm BiSb-layer and a compressive stress of -4 MPa for the 150 nm Sb-layer was determined. In the mechanical simulation the values of the intrinsic stress of the BiSb- as well as Sb-layer were kept constant. Values for Young's modulus  $E$  and Poisson's ratio  $\nu$  are [10]:

$$\text{Bi: } E=32 \text{ GPa } \nu=0.33 \quad \text{Sb: } E=55 \text{ GPa } \nu=\text{n.a.}$$

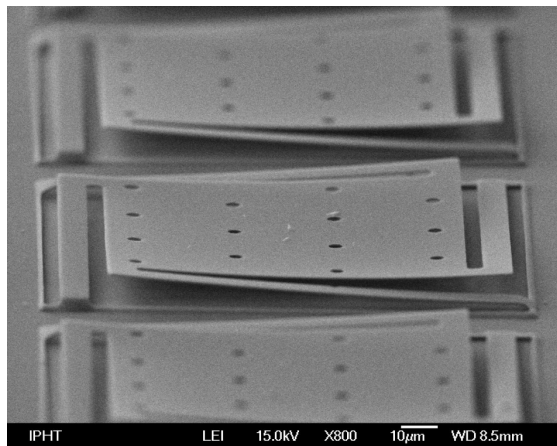
An exact value for Young's modulus as well as Poisson's ratio of  $\text{Bi}_{0.87}\text{Sb}_{0.13}$  was not available in the literature. It seems to be justified, however, to use the values of pure Bi instead of BiSb due to the dominant proportion of Bi in the  $\text{Bi}_{0.87}\text{Sb}_{0.13}$  alloy.

Upon the  $\text{Si}_x\text{N}_y$  passivation layer a 80 nm thin NiCr layer was deposited and patterned in a wet etch process against a AZ5214E photoresist mask. Afterwards the photoresist was completely removed in acetone. For structuring of the  $\text{Si}_x\text{N}_y$  membrane the same RIE-ICP reactive dry etch process with  $\text{CHF}_3/\text{CF}_4/\text{He}$  as described above was applied.

Due to the high selectivity of the RIE process compared to organic layers the etch process stops onto the polyimide surface. In an anisotropic RIE oxygen-plasma process the exposed polyimide regions were structured 2.5  $\mu\text{m}$  perpendicularly, followed by an isotropic remote RIE oxygen process, which removes the sacrificial layer completely.

## 2.5 Absorber types

The FPA can be equipped with two different absorber types, a quarter wavelength absorber (QWA) as well as a colloidal silver black layer. In the case of the QWA a 80 nm thin gold reflector layer has to be structured beneath the sacrificial layer. In combination with the freestanding membrane an optical resonator structure with an appropriate  $\lambda/4$  optical distance will be obtained. The absorption properties can be improved by a deposition of a very thin metal layer upon the absorber area [6]. In preliminary tests freestanding membranes were deposited with a variation of very thin NiCr layers, as it is presented in Fig.4. The highest integral absorption coefficient  $\alpha$  of about 0.88 in the range from 8-14  $\mu\text{m}$  was obtained with a



sheet resistance  $R=192 \Omega$ . This value approximates the half of the free space impedance of vacuum  $Z_0 = (\mu_0/\epsilon_0)^{1/2} = 377 \Omega$  [6] being the theoretical prediction for maximum absorption. The influence of the NiCr thickness on the absorption characteristic is presented in Fig.5. All absorption spectra were measured with the IR-Microscope UMA 500 of the FTIR-Spectrometer Bio-Rad Excalibur.

Fig.4: Freestanding perforated membranes used for preliminary tests of absorption characteristics with different NiCr thickness.

An alternative absorber is the colloidal silver black layer. This layer has a fluffy structure with several microns in thickness. Its adhesive strength to the membrane is sufficient. The colloidal layer was deposited by a thermal evaporation process in a vacuum chamber under reduced atmosphere. Advantageously an accordingly designed punch mask is aligned over the substrate and fixed both together.

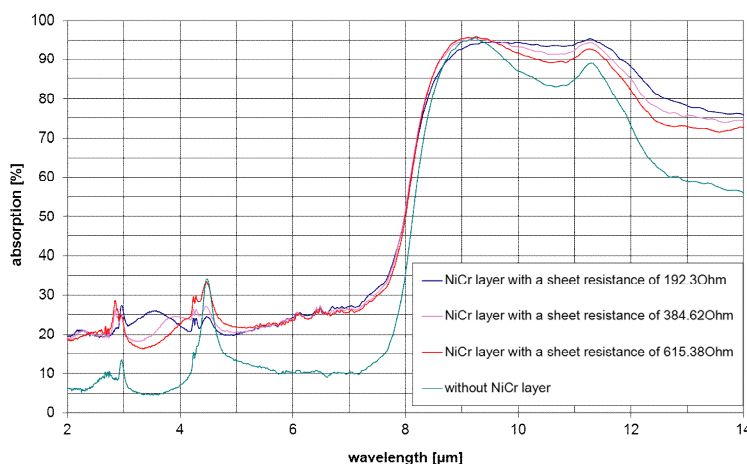


Fig.5: Infrared absorption spectra of the QWA with a variation of NiCr layer sheet resistance corresponding to a variation in NiCr thickness.

Instead of silver it is possible to use gold to obtain an analogous colloidal gold black layer with a similarly high absorption efficiency [5]. However, the absorption efficiency depends on the thickness of the colloidal black layer, which is regulated by the amount of evaporated material. Due to the high absorption coefficient of nearly 100 % over a broad wavelength interval, this absorber type is well applicable for spectral measurements.

### 3. Results of an equivalent test structure

The test structure was fabricated in bulk-micromachining and presents the latest state of development of the preliminary tests. It has the same geometry parameters as the final pixel structure in surface-micromachining and is, therefore, fully comparable from the thermal point of view:

absorption area:	(100 x 100) $\mu\text{m}^2$
width of spiral legs:	10 $\mu\text{m}$
width of thermoelectric legs:	2 $\mu\text{m}$

Due to the longer fabrication time and process chain of surface-micromachined structures compared to the bulk-micromachined, first measurement results of signal voltage obtained by using an infrared source were determined by the characterization of the equivalent test structure.

The absorber is based on a stack of 0.8  $\mu\text{m}$   $\text{Si}_x\text{N}_y$ , 1  $\mu\text{m}$  SU8 and a NiCr layer with a sheet resistance of 460  $\Omega/\square$ . The absorption coefficient was determined by FTIR measurements to be 52%. By contrast, the non-completed final structure in surface micromachining combined with a silver black layer absorber, will obtain an absorption coefficient of nearly 100%, as it is described in chapter 2.5. Based on the linear correlation between the signal voltage and the absorption coefficient, the measured results of the test structure were converted directly into the expected results of the final structure under the same measurement conditions.

The signal voltage was measured in front of a black body source generating an irradiance of 38  $\text{W}/\text{m}^2$ . At normal pressure atmosphere a signal voltage of 10  $\mu\text{V}$  was measured, which increased under vacuum condition to 464  $\mu\text{V}$  resulting in a detectivity of  $6 \cdot 10^8 \text{ cmHz}^{1/2}/\text{W}$  under consideration of the 52 % of absorption. The thermal time constant was measured to be 36 ms, again under vacuum conditions.

Due to the very positive preliminary test a detectivity of  $1.2 \cdot 10^9 \text{ cmHz}^{1/2}/\text{W}$  was pre-estimated for the final structure with a silver black layer and an absorption coefficient of nearly 100%.

### 4. Conclusions

The fabrication of a FPA by using surface-micromachining with different absorber types was presented. The technical difficulties of realizing stress-controlled free-standing  $\text{Si}_x\text{N}_y$  membranes were described. The applicability of a quarter wavelength absorber with  $\alpha \approx 88\%$  as well as a colloidal silver black layer with  $\alpha \approx 100\%$  was demonstrated. An equivalent bulk micromachined test structure with accurate the same geometric dimensions as the final structure fabricated by surface micromachining was characterized. It was pre-estimated to achieve a detectivity of  $1.2 \cdot 10^9 \text{ cmHz}^{1/2}/\text{W}$  by using a colloidal silver black layer in combination with the surface micromachined structure.

### Acknowledgement

This work was funded by the Bundesministerium für Bildung und Forschung (BMBF), project VISA, GrantNo. 16SV2286.

### References

- [1] M.C. Foote et al., Thermopile detector arrays for space science applications, *Proceedings of the International Workshop on Thermal Detectors for Space Based Planetary, Solar, and Earth Science Applications*, 2003, pp. 2-16 – 2-20.
- [2] M. Hirota et al., 120x90 element thermoelectric infrared focal plane array with precisely patterned Au-black absorber, *Sensors and Actuators A*, **135** (2007) 146-151.
- [3] A. Schaufelbühl et al., Uncooled low-cost thermal imager based on micromachined CMOS integrated sensor array, *J. Microelectromech. Systems*, **10** (2001) 503-510.
- [4] R. A. Wood, Uncooled thermal imaging with monolithic silicon focal plane arrays, *Proc. SPIE*, **2020** (1993) 322-329.
- [5] W. Becker et al., Black gold deposits as absorbers for far infrared radiation, *Phys. Status Solidi B* **194** (1996) 241-255.
- [6] A. Hadni et al., Infrared and millimeter wave absorber structures for thermal detectors, *Infrared Phys.* **30** (1990) 465-478.
- [7] J. Lehman et al., Very black infrared detector from vertically aligned carbon nanotubes and electric-field poling of lithium tantalate, *Nano Lett.* (2010) DOI: 10.1021/nl100582j.
- [8] T. Elbel, *Mikrosensorik, 1. Edition, Vieweg-Verl.*, 1996.
- [9] F. Völklein and E. Kessler, Thermal conductivity and thermoelectric figure of merit of  $\text{Bi}_{1-x}\text{Sb}_x$  films with  $0 < x < 0.3$ , *Phys. Status Solidi B* **143** (1987) 121-130.
- [10] G.W.C.Kaye and T.H.Laby, *Tables of physical and chemical constants*, Longman, London, UK, 15th edition, 1993.